Incidence Angle Correction of AirSAR Data to Facilitate Land-Cover Classification

Carl H. Menges, Greg J.E. Hill, Waqar Ahmad, and Jakob J. van Zyl

Abstract

Three image-based methods for correcting the effect of changes in incidence angle on backscatter data are proposed and evaluated for AirSAR data of a coastal tropical savanna landscape in Australia's Northern Territory. These correction methods require little field knowledge and do not assume a linear relationship between SAR backscatter and incidence angle. The correction methods are applied to five independent components of the Stokes Matrix. The results are evaluated using an existing land-cover classification to extract mean backscatter values for individual land-cover classes before and after the correction procedures. It is shown, for the vegetation communities involved, that the slope method provides a successful correction for the amplitude components of the backscatter data. The real and imaginary parts of the co-polarized returns are best corrected using the LUT method. The proposed correction procedure allowed the use of a maximum-likelihood classification for the discrimination of ten land-cover types with an overall accuracy of 87 percent across the complete swath width of the AirSAR data.

Introduction

The ability of Synthetic Aperture Radar (SAR) to image the Earth's surface independently of cloud cover and sun illumination at a resolution comparable to that of optical instruments makes this a valuable tool for the tropical regions around the globe. Microwave systems also provide different information from that of optical sensors because the scattering process is influenced by the structural elements of the land cover rather than their chemical composition.

During the 1996 NASA/JPL Airborne Imaging Radar (AirSAR) mission, which involved Australia, New Zealand, Malaysia, the Philippines, and the United States, multifrequency (C-, L-, and P-band), quad-polarized SAR data were acquired for a study area in the tropical savanna of northern Australia. The aim of the project was to evaluate the utility of these data for the mapping and monitoring of vegetation communities typical of the study area. Conventional image classification techniques cannot be applied to SAR data because the backscatter is not only dependent on the ground cover but also on the incidence angle of the radar waves relative to the ground. In the range direction, perpendicular to the flight path, the look angle ranges from 20 to 60 degrees.

Backscatter from natural surfaces is an interaction between microwave radiation and tree canopies, understorys, and ground layers as functions of incidence angle, wavelength, and polarization (Wang *et al.*, 1993a; Wang *et al.*, 1993b). The effect of variation in incidence angle can be modeled if the composition of ground cover is known as the behavior varies for different scattering mechanisms (Wang *et al.*, 1997; Champion, 1996; Lin *et al.*, 1994; Wang *et al.*, 1993a; Wang *et al.*, 1993b; Bertuzzi, 1992; Sun *et al.*, 1991; Engman, 1991; Sun and Simonett, 1988). The "incidence angle" is defined as the angle between the radar line-of-sight and the local vertical with respect to the geoid (Henderson and Lewis, 1998).

Most researchers attempting to extract information content from radar data using digital image processing have confined their study to a limited range of incidence angles, typically spanning approximately 10 degrees (Rignot *et al.*, 1994a; Israelsson *et al.*, 1994; Dobson *et al.*, 1992; Hussin *et al.*, 1991). It is argued that the effect of incidence angle in this limited range does not cause significant changes in backscatter characteristics. A correction for the effects of incidence angle has been proposed based on a linear regression of backscattering intensities versus incidence angle for a single cover type (Baker *et al.*, 1994; Ranson and Sun, 1994). Due to the effect being different for differing land-cover components, such a correction is only valid for the cover type from which the regression was derived. Maximum-likelihood approaches have been used with high land-cover discrimination accuracy for given study areas (Ranson and Sun, 1997; Saatchi *et al.*, 1997; deGrandi *et al.*, 1994; Lemoine *et al.*, 1994; Ranson and Sun, 1994; Rignot *et al.*, 1994b). Decision trees (Hess *et al.*, 1995), fuzzy classifiers (Du and Lee, 1996), and image segmentation (Rignot and Chellappa, 1992; Dong *et al.*, 1998) have also been used for image analysis. Significant variation of backscatter intensities due to changes in incidence angle make these approaches unsuitable because they are based on a comparison of pixel values, or area statistics in the case of image segmentation.

Menges *et al.* (1998) investigated the relationship between AirSAR backscatter components and changing incidence angle for land-cover types of the tropical savannas of northern Australia. This study confirmed that the effect of changing incidence angles is dependent on the land cover present as is expected from theoretical models. In the present study, three image-based methods are proposed and evaluated for the correction of incidence angle effects in AirSAR data. All three methods are based

C.H. Menges, G.J.E. Hill, and W. Ahmad are with the Faculty of Science, Northern Territory University, Darwin, NT 0909, Australia (carl@gis.ntu.edu.au).

J.J. van Zyl is with the Jet Propulsion Laboratory, California Institute of Technology, 4800 Oak Grove Drive, Pasadena, CA 91109.

Photogrammetric Engineering & Remote Sensing
Vol. 67, No. 4, April 2001, pp. 479–489.

0099-1112/01/6704–479$3.00/0

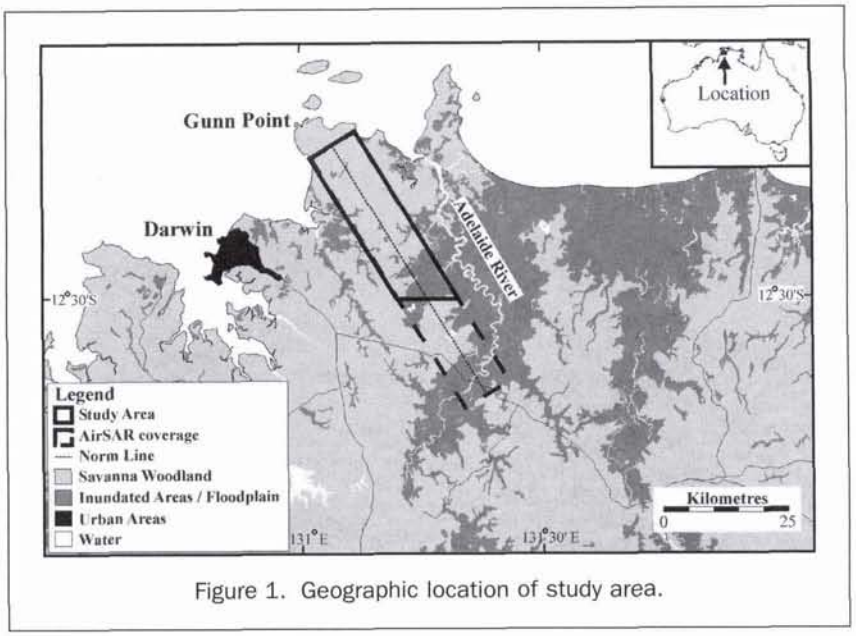

Figure 1. Geographic location of study area.

on the premise that all "azimuth lines," lines parallel to the flight line with constant incidence angle, contain a similar range of land cover. That is, as seen in Figure 1, all lines parallel to the norm line have a similar proportion of inundated area or floodplain and savanna, which are the key cover types in the study area. The correction is then achieved by a histogram equalization between every azimuth line and the norm line. Histogram equalization is a common method applied for the radiometric calibration of optical data for the purpose of change detection or image mosaicking (Jensen, 1986; Chavez and MacKinnon, 1994; Um and Wright, 1999). The proposed methods use three different implementations of the histogram matching between lines of constant incidence angle: The LUT (Look-Up-Table) method matches the cumulative distribution of the norm line directly for each azimuth line. The "Line-of-Best-Fit" method uses the parameters of a linear regression between an azimuth line and the norm line to facilitate a correction. The third method is similar to the previous but only uses the slope of this regression for the correction process. Finally, an image classification over the complete swath width of the incidence angle corrected AirSAR data is carried out.

Study Area

The savannas of northern Australia occupy approximately 20 percent of the Australian continental landmass and lie within the wet tropical bioclimatic. The climate of the study site in the Darwin region is tropical, characterized by the summer monsoon, which brings torrential rains generally between December and March. The average annual rainfall is 1600 mm. While humidity levels range from an average of 75 percent during the wet to 50 percent in the dry season, the mean maximum temperature in the area exhibits little variation, ranging from 35°C to 31°C in the respective seasons (Hickey, 1985). Distinct rainfall, temperature, and humidity variation within these periods has created a diverse assemblage of savanna vegetation in northern Australia. This varies from well vegetated areas to sparsely vegetated areas, and the composition and structure appears to be governed to a large extent by soil water availability and to a lesser extent nutrient availability (Wilson *et al.*, 1990).

The study area is approximately 50 km northeast of Darwin (130° 45′ E, 12° 30′ S) in the Northern Territory (Figure 1) and is a typical tropical savannas forest site representative of northern Australia. Recently acquired digital and ancillary data such as ground survey data, vegetation type, and land system/units maps are available. This area contains a wide range of tree species such as *Eucalyptus miniata, Eucalyptus tetrodonta, Erythrophleum chlorostacys, Melaleuca cajuputi and viridiflora*, and *Callitris intratropica*. The vegetation communities, characterized by the dominant species, range from open woodland to closed forests but are dominated by *Eucalypt* open forest. The study area also encompasses part of the Adelaide River and associated floodplains. These are seasonally inundated grass and sedgeland with little or no woody vegetation. The introduced woody weed *Mimosa pigra* is an exception. This weed is found throughout the wetlands of the Northern Territory including the Adelaide River floodplain contained in the study area. The topography of the study area is flat with elevation above sea level ranging from 0 to 31 meters.

Data and Methodology

The JPL AirSAR system was flown over the study site on board a DC-8 aircraft on 23 November 1996. The AirSAR acquired backscatter data at C-band (wavelength = 5.6 cm, frequency = 5.3 Ghz), L-band (23.9 cm, 1.25 Ghz), and P-band (67.0 cm, 0.44 Ghz) in four transmit/receive polarizations (HH, VV, HV, VH). Local time of data acquisition was 1100 hours under dry weather conditions with some cloud present. The AirSAR data (as shown in Plate 1) were processed as a 60-km strip product by JPL's Radar Data Center using Version 6.1 of the integrated processor, and were supplied in 18-look compressed Stokes matrix format. The look angle ranges from 22.6 degrees to 61.7 degrees in the range direction.

The Stokes Matrix for polarimetric SAR data is a 4 by 4 matrix (van Zyl and Ulaby, 1990). Due to the assumption of symmetry (i.e., $S_{hv} = S_{vh}$) and averaging as part of the multilook processing, a maximum of nine independent numbers need to be stored for each image pixel (Zebker and van Zyl, 1991). The compressed Stokes Matrix as processed by JPL's Radar Data Center, therefore, contains ten bytes of information per pixel, with two bytes being used to store the total power.

Nine independent elements describing the scattering behavior can be extracted for each frequency (see Table 1). Five of these components that contain valuable information (Baker *et al.*, 1994) are considered here: the three bands containing the magnitude of the backscatter at HH, VV, and HV polarization as well as the real and imaginary component of the co-polarized

TABLE 1. ELEMENTS OF THE SCATTERING MATRIX EXTRACTED FROM THE COMPRESSED STOKES MATRIX FORMAT

Scattering Element	Description
$\langle S_{HH}S_{HH}^* \rangle$	Magnitude of HH return
$\langle S_{VV}S_{VV}^* \rangle$	Magnitude of VV return
$\langle S_{HV}S_{HV}^* \rangle$	Magnitude of HV return
$Re\langle S_{HH}S_{VV}^* \rangle$	Real part of HH-VV co-polarized return
$Im\langle S_{HH}S_{VV}^* \rangle$	Imaginary part of HH-VV co-polarized return
$Re\langle S_{HH}S_{HV}^* \rangle$	Real part of HH-HV cross-polarized return
$Im\langle S_{HH}S_{HV}^* \rangle$	Imaginary part of HH-HV cross-polarized return
$Re\langle S_{HV}S_{VV}^* \rangle$	Real part of HV-VV cross-polarized return
$Im\langle S_{HV}S_{VV}^* \rangle$	Imaginary part of HV-VV cross-polarized return

backscatter. The latter two components can be used to compute the HH-VV phase difference and the correlation coefficient.

In this study the AirSAR data were used in slant range resolution to avoid the introduction of an additional dependence of the data on range location and thus incidence angle. The incidence angle was assumed to be determined by the range location alone due to negligible topographic variation within the study area.

Three methods were implemented to correct the data to a nominal incidence angle. All methods rely on the comparison of individual azimuth lines to the azimuth line located at a nominal incidence angle (48 degrees), hitherto referred to as the "norm line." This value was chosen on the basis that the assumption, on which the three methods are based, that each azimuth line has a similar distribution of land cover has greater validity if the reference line is near the center of the image. This is mainly due to the floodlain contained in the image, which occupies increasing proportions of the azimuth lines with larger incidence angles (see Figure 1). A second reason for placing the norm line at the center of the image is that the difference between backscattering behavior of different land covers at incidence angles between 40 and 50 degrees appears to be maximal in the study area (Menges *et al.*, 1998). Before the regression of an azimuth line versus the norm line, the data are numerically sorted to generate a frequency distribution. The correction procedures are based on and applied to the 6550 rows of data available in the 60-km flight strip, and all calculations were performed using floating point intensity data.

The LUT method utilizes the numerically sorted norm line data as a look up table to determine the corrected values for other azimuth lines (Menges *et al.*, 2001a). The method operates on a pixel-by-pixel basis on the AirSAR data. For each pixel, the first step is to identify the level of backscatter relative to all other values occurring at the same incidence angle. This was achieved by numerically sorting the line data and calculating the cumulative frequency of the value's occurrence for that particular azimuth line. As a second step, the backscatter value associated with this cumulative frequency in the norm line was determined and written to the "corrected" image.

The Line-of-Best-Fit method involved the determination of a line of best fit between each numerically sorted azimuth line and the norm line. The slope and offset of this line of best fit at a specific incidence angle was then applied to the data within this azimuth line. The validity of assuming a linear relationship between the numerically sorted azimuth lines and the norm line was tested for each channel of the data set using an arbitrarily determined azimuth line in the near and far range.

The Slope method was identical to the second, with the exception that only the slope of the line of best fit was used for the determination of the "corrected" values. The offset was ignored.

Verification of the results of these procedures was undertaken by extracting the average backscatter values of known land-cover classes from the corrected data and plotting these against incidence angle. The land-cover classes were derived by classification of Landsat TM data acquired in April 1996 (Ahmad *et al.*, 1998).

In order to facilitate the extraction of backscatter values according to land-cover classes, the classified TM data were registered to the SAR data using the following procedure. The classified Landsat TM data were available as a georeferenced image with a pixel size of 30 by 30 m. To transfer this image to the geometry of the raw AirSAR data, it was converted to a slant range projection. The image was first rotated by 31.4 degrees in a clockwise direction to account for the AirSAR flight heading of 148.6 degrees. Second, a subset was taken from the rotated image by means of visually identifying the extent of the AirSAR data. The subset at this stage included a spatial extent similar to that of radar data, and the pixel and line directions were identical. Third, the subset was converted into slant range, calculating the local incidence angle according to the acquisition parameters of the AirSAR data. The slant range pixel size at this stage was chosen as 10 m, such that each original pixel was represented at least once in the resulting image. A slant range pixel of 10 m at the minimum incidence angle equates to a ground range pixel size of less than 30 m. As a final step, the image was registered to the AirSAR data using 20 control points at an RMS error of less than one pixel. Resampling at all stages of the process was carried out using a first-order polynomial equation and the nearest-neighbor algorithm.

Two land-cover types were selected for the evaluation procedure. Eucalypt Woodland contained the vegetation communities *Eucalyptus miniata/tetrodonta* open forest, *Eucalyptus tetrodonta* forest, and *Eucalyptus bleeseri/tetrodonta* woodland. These were found to be highly similar in their scattering properties (Menges *et al.*, 1998) and are the dominant vegetation communities in the study area. The second land-cover class was Floodplain, which was found to behave in a manner quite different from the Eucalypt Woodland communities (Menges *et al.*, 1998). For these two land-cover classes, average AirSAR data values were extracted according to the local incidence angle for each band. The local incidence angle was calculated according to the range location and rounded to the nearest whole integer, resulting in one-degree intervals for which the mean data value was calculated.

An image classification was implemented using the incidence angle corrected AirSAR data. The magnitude of the HH, VV, and HV channels in all three bands was corrected using the slope method, and the real and imaginary components of the HHVV co-polarized returns of all bands were corrected using the Line-of-Best-Fit method. The VV polarization for all bands and the imaginary part of L-HHVV were excluded from the classification because these did not contribute to the class separability. This was determined by a separability analysis of training areas using the transformed divergence measure (Menges *et al.*, 1999). A maximum-likelihood algorithm was chosen for the classification with a 5 percent probability threshold.

Because the maximum-likelihood classifier is based on the assumption of normal distribution within training samples, the magnitude channels were transformed to a logarithmic scale, that is, to decibel values. A mean 3 by 3 filter was applied to all channels before this logarithmic transformation to reduce the effective resolution of the data, approximating the optimal resolution for the detection of these ecological units (Menges *et al.*, 2001b) and to reduce the speckle. The data are supplied by JPL as an 18-look average. Calculation of the Equivalent Number of Looks (ENL) as the ratio of the square of the mean divided by the variance for a homogeneous distributed target resulted in a value of 6.3 for the raw data. The ENL for the mean filtered intensity data equals 26.4 using the same target. The data were georeferenced to a 1:50,000-scale topographic map with less than one-pixel error and resampled to a 10- by 10-meter resolu-

TABLE 2. CORRELATION COEFFICIENTS FOR THE LINEAR REGRESSION OF TWO RANDOMLY CHOSEN LINES IN THE NEAR (33 DEGREES INCIDENCE ANGLE) AND FAR RANGE (60 DEGREES INCIDENCE ANGLE) VERSUS THE NORM LINE. THE VALUES OBTAINED AT ALL THREE FREQUENCY BANDS AVAILABLE FOR THE FIVE SCATTERING ELEMENTS ARE SHOWN.

Near Range Line vs Norm Line				Line 2300 vs Norm Line			
Band	C	L	P	Band	C	L	P
$\langle S_{HH}S_{HH}^* \rangle$	0.9988	0.9942	0.9943	$\langle S_{HH}S_{HH}^* \rangle$	0.9971	0.9891	0.9899
$\langle S_{VV}S_{VV}^* \rangle$	0.9983	0.9946	0.9986	$\langle S_{VV}S_{VV}^* \rangle$	0.9980	0.9915	0.9952
$\langle S_{HV}S_{HV}^* \rangle$	0.9989	0.9967	0.9974	$\langle S_{HV}S_{HV}^* \rangle$	0.9971	0.9877	0.9902
$\mathrm{Re}\langle S_{HH}S_{VV}^* \rangle$	0.9975	0.9935	0.9975	$\mathrm{Re}\langle S_{HH}S_{VV}^* \rangle$	0.9960	0.9238	0.9753
$\mathrm{Im}\langle S_{HH}S_{VV}^* \rangle$	0.9991	0.9962	0.9938	$\mathrm{Im}\langle S_{HH}S_{VV}^* \rangle$	0.9996	0.9788	0.9287

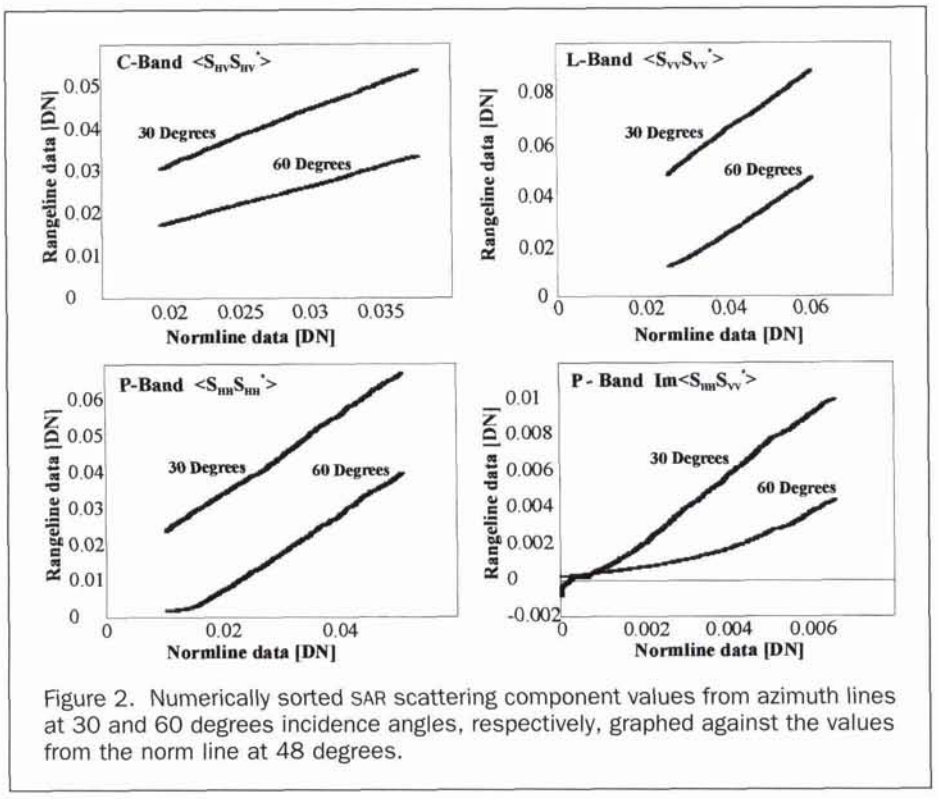

Figure 2. Numerically sorted SAR scattering component values from azimuth lines at 30 and 60 degrees incidence angles, respectively, graphed against the values from the norm line at 48 degrees.

tion to allow the evaluation of the classification against ground data.

Results

A comparison of the norm line values with arbitrarily chosen azimuth lines in the near and far range was used to determine the validity of applying a linear regression to the data sets. The numerically sorted data in the lines to be regressed was found to have very high correlation coefficients (see Table 2). For the azimuth lines in the near range, at an incidence angle of 33 degrees, the correlation coefficients exceeded 0.99 for all scattering components. The lowest value for the azimuth lines tested, at an incidence angle of 60 degrees, was 0.9238 for the real part of the HHVV co-polarized return in the L-Band.

A graphical representation of some of the relationships between the two azimuth lines tested and the norm line is shown as a crossplot in Figure 2. Three examples have been chosen for backscatter magnitude components and one for the components of the HHVV co-polarized return. The examples chosen are typical of the relationships observed. For the azimuth line data with an incidence angle of 60 degrees, the relationships show non-linear behavior at very low data values. The extent of this curvature varies between scattering elements and frequency bands but is present throughout.

Results of the correction procedures applied to the SAR data are shown in Tables 3 to 5 for the C-, L-, and P-Bands, respectively, as well as in Figures 3 to 6. Each of the tables consists of two parts divided by the two land-cover types used in the evaluation. For each cover type, the correlation coefficient and slope of a linear regression between incidence angle and observed data values derived from raw data and each of the three correction methods is given. The results for the LUT and Line-of-Best-Fit methods of correction are very similar as should be expected if there is a strong linear relationship present between sorted azimuth lines. Due to the strong similarity, the two methods will not be discussed separately. Any further reference to the LUT method will imply the same comment or result for the Line-of-Best-Fit method.

Figure 3 contains five graphs for the respective channels in the C-Band. The incidence angle is graphed on the *x*-axis in degrees. The *y*-axis covers the range of data values (Intensity for magnitude of HH, VV, and HV backscatter) present in the channel for raw data, the LUT correction, and the Slope-correction method. The data values are the average of data values observed at each incidence angle within pixels designated as Eucalypt Woodland communities by the Landsat TM classification of the study area. The angular dependence of the raw data can be clearly seen. The HH polarization data are well repre-

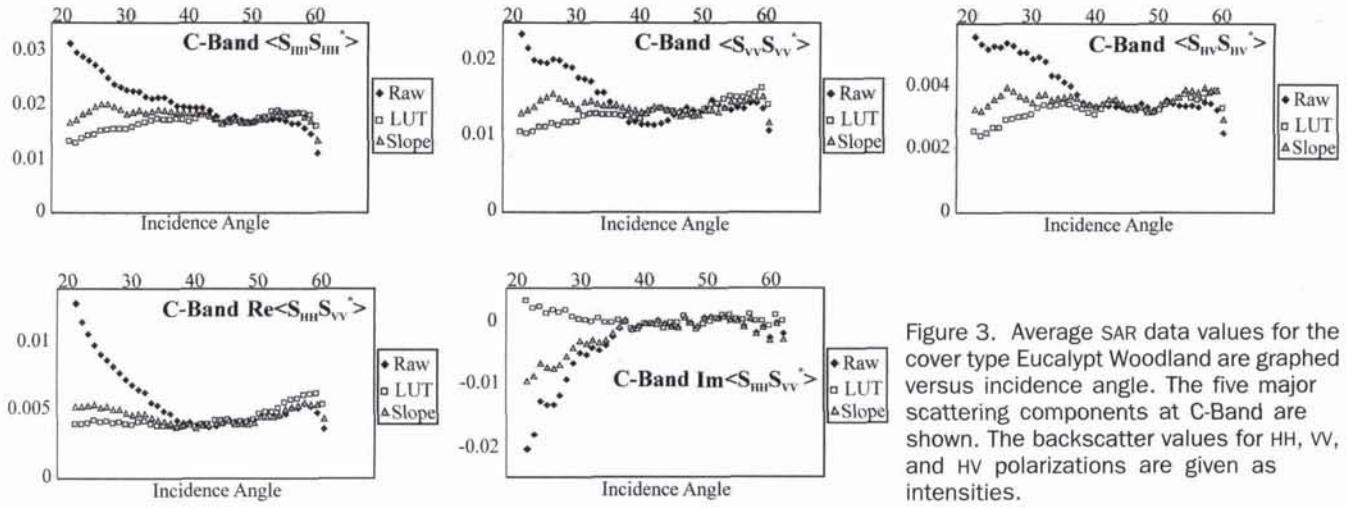

Figure 3. Average SAR data values for the cover type Eucalypt Woodland are graphed versus incidence angle. The five major scattering components at C-Band are shown. The backscatter values for HH, VV, and HV polarizations are given as intensities.

TABLE 3. THE CORRELATION COEFFICIENTS AND SLOPE FOR THE LINEAR REGRESSION OF C-BAND SAR DATA VS INCIDENCE ANGLE FOR TWO DOMINANT LAND-COVER TYPES OF THE STUDY AREA.

E. Woodland Communities at C-Band

Scattering Element	Raw Data		LUT Method		Line-of-Best-Fit Method		Slope Method	
	r	slope	r	slope	r	slope	r	slope
$\langle S_{HH}S_{HH}^* \rangle$	−0.95	−0.075757	0.81	0.028464	0.84	0.031265	−0.49	−0.012679
$\langle S_{VV}S_{VV}^* \rangle$	−0.74	−0.055888	0.93	0.038728	0.93	0.040089	−0.23	−0.005005
$\langle S_{HV}S_{HV}^* \rangle$	−0.90	−0.067980	0.80	0.032806	0.81	0.034829	0.02	0.000544
$Re\langle S_{HH}S_{VV}^* \rangle$	−0.74	−0.000146	0.76	0.000048	0.76	0.000052	−0.11	−0.000006
$Im\langle S_{HH}S_{VV}^* \rangle$	0.76	0.000035	−0.43	−0.000004	−0.43	−0.000003	0.74	0.000018

Floodplain at C-Band

Scattering Element	Raw Data		LUT Method		Line-of-Best-Fit Method		Slope Method	
	r	slope	r	slope	r	slope	r	slope
$\langle S_{HH}S_{HH}^* \rangle$	−0.93	−0.079532	0.53	0.023385	0.56	0.027297	−0.40	−0.016936
$\langle S_{VV}S_{VV}^* \rangle$	−0.72	−0.059588	0.65	0.034903	0.66	0.037474	−0.21	−0.008991
$\langle S_{HV}S_{HV}^* \rangle$	−0.85	−0.068291	0.57	0.033322	0.58	0.036193	0.00	0.000148
$Re\langle S_{HH}S_{VV}^* \rangle$	−0.70	−0.000138	0.63	0.000053	0.66	0.000057	0.00	0.000000
$Im\langle S_{HH}S_{VV}^* \rangle$	0.65	0.000038	0.05	0.000002	0.08	0.000002	0.58	0.000023

sented as a linear relationship with a correlation coefficient of −0.95 (Table 3). According to this regression, a 10-degree change of incidence angle causes a difference of 0.8 decibels in backscatter. The VV, HV, and real part of the co-polarized return data exhibit an inverse relationship with incidence angle below 40 degrees. In the range of 40 to 60 degrees there is little change with angular variation, followed by a rapid decrease in the very far range. The imaginary part of the co-polarized return is positively related to the incidence angle and also shows little variation above a 40-degree incidence angle.

The data values derived from the LUT correction reduce the angular dependence in the C-Band significantly, but there is a tendency for "over-correction." That is, the LUT-corrected data retains a dependency to incidence angle opposite to that of the raw data. For a linear regression (Table 3) fit to the C-HH data of *Eucalypt* Woodland communities, for example, the LUT correction reduces the absolute value of the correlation coefficient from 0.95 to 0.81 (0. 84) with a change in sign. Similarly, the slope is reduced in absolute value from 0.076 to 0.028 (0.031) with a change in sign. The other scattering components behave very similarly for both cover types, with the exception of the Imaginary part of HHVV for the Floodplain, where no change of sign occurs.

The Slope-corrected data have the least dependence to incidence angle for all channels, except for the Imaginary part of the co-polarized return, as measured by the correlation coefficient of a linear fit. Equally, the slope values have the least magnitude with the same exception. The graphical representation (Figure 3) supports this finding, with the Slope-corrected data showing least dependence on incidence angle. For the imaginary part of HHVV, the LUT-corrected data still appears to have "over" corrected in the near range, but the Slope method has failed to achieve sufficient correction.

Figure 4 and Table 4 contain the results for the evaluation of the correction procedures in the L-Band. The effect of the correction methods is very similar to that observed at the C-Band, but less pronounced. The correlation coefficients for a regression are substantially lower, indicating that the variation

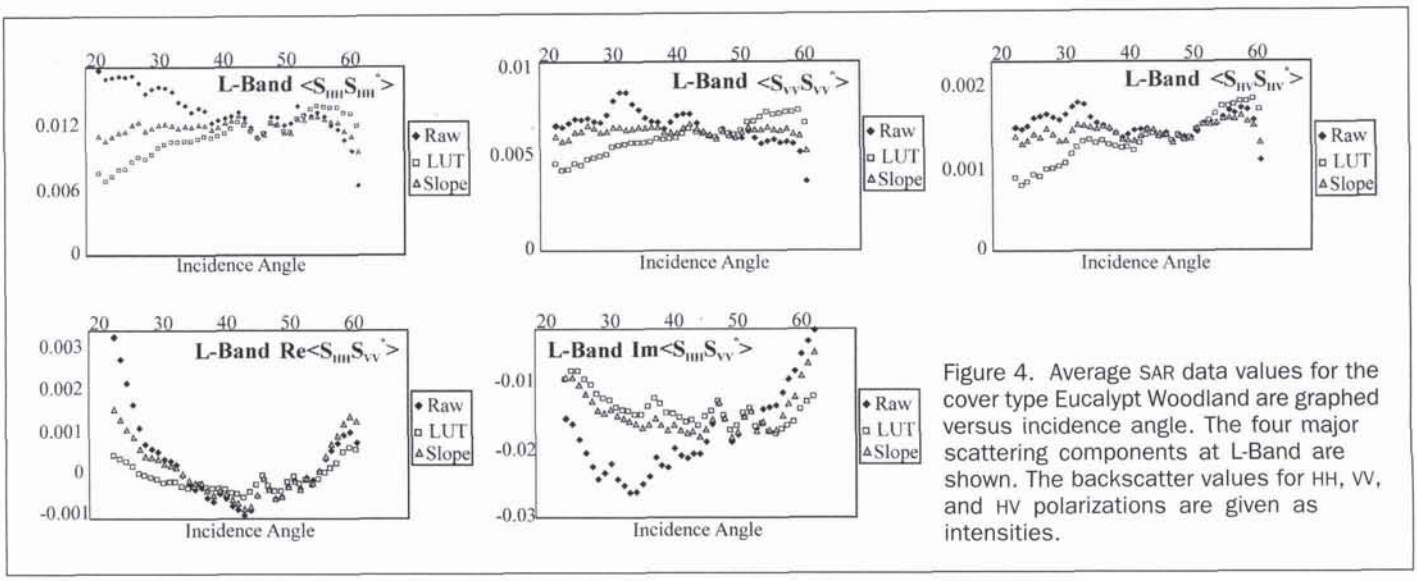

Figure 4. Average SAR data values for the cover type Eucalypt Woodland are graphed versus incidence angle. The four major scattering components at L-Band are shown. The backscatter values for HH, VV, and HV polarizations are given as intensities.

TABLE 4. THE CORRELATION COEFFICIENTS AND SLOPE FOR THE LINEAR REGRESSION OF L-BAND SAR DATA VERSUS INCIDENCE ANGLE FOR TWO DOMINANT LAND-COVER TYPES OF THE STUDY AREA.

E. Woodland Communities at L-Band

Scattering Element	Raw Data		LUT Method		Line-of-Best-Fit Method		Slope Method	
	r	slope	r	slope	r	slope	r	slope
$\langle S_{HH}S_{HH}^* \rangle$	−0.81	−0.054494	0.92	0.063211	0.92	0.066976	0.12	0.002611
$\langle S_{VV}S_{VV}^* \rangle$	−0.72	−0.039150	0.95	0.057229	0.95	0.056865	−0.13	−0.002126
$\langle S_{HV}S_{HV}^* \rangle$	−0.23	−0.008164	0.94	0.078725	0.93	0.076216	0.45	0.010797
$Re\langle S_{HH}S_{VV}^* \rangle$	−0.38	−0.000032	0.11	0.000003	0.14	0.000006	−0.11	−0.000007
$Im\langle S_{HH}S_{VV}^* \rangle$	0.77	0.000040	−0.67	−0.000014	−0.60	−0.000015	0.02	0.000001

Floodplain at L-Band

Scattering Element	Raw Data		LUT Method		Line-of-Best-Fit Method		Slope Method	
	r	slope	r	slope	r	slope	r	slope
$\langle S_{HH}S_{HH}^* \rangle$	−0.70	−0.040846	0.85	0.075353	0.85	0.082233	0.37	0.015403
$\langle S_{VV}S_{VV}^* \rangle$	−0.57	−0.032264	0.85	0.061330	0.85	0.063642	0.12	0.003999
$\langle S_{HV}S_{HV}^* \rangle$	−0.06	−0.027778	0.84	0.081504	0.83	0.081381	0.37	0.015626
$Re\langle S_{HH}S_{VV}^* \rangle$	−0.39	−0.000037	0.01	0.000001	0.14	0.000007	−0.09	−0.000005
$Im\langle S_{HH}S_{VV}^* \rangle$	0.41	0.000027	−0.57	−0.000024	−0.58	−0.000025	−0.24	−0.000010

of backscatter with incidence angle is not well described by a linear function. The reduction in the correlation coefficient achieved by the correction methods can, however, still be seen as an indication that the dependence of backscatter values on incidence angle has decreased although the graphical representation must be taken into consideration. From the graphs (Figure 4) it can be seen that the Slope-correction method results in values between raw data and those derived from the LUT correction. The Slope correction also achieved the lowest correlation coefficients (Table 4) with the exception of L-HV, where correlation and slope of the raw data were lower than that of the corrected data (see Table 4). The graph, however, demonstrates the effectiveness of the Slope correction. In the raw data, there is a peak between a 30 and 40 degrees incidence angle and there is a rapid decline in values at 60 degrees. The Slope-correction method reduces both these phenomena, which should not occur because these values are derived from a single cover type for all incidence angles. The least successful correction by the Slope method occurred for the real part of the HHVV co-polarized return. Here, the raw data have a relationship to incidence angle that would be better described by a second-order polynomial. The Slope correction results in a decrease of the values in the near range, but produces even higher values in the far range than are present in the raw data. The LUT method is the most successful in reducing the effect of incidence angle for this case. Similarly, the LUT method achieves a better result in correcting the imaginary component of the co-polarized return in the far range, above 50 degrees.

In the P-Band (see Figure 5 and Table 5) the effects of the correction methods are least effective because the effects of incidence angle variation on backscatter are smallest in this Band. A significant reduction in overall slope can only be observed for the VV polarization. The effect in HH and HV is a reduction of peaks and troughs within the raw data, which is a benefit of the correction procedure because these should not exist for a single cover type. This benefit is not reflected in the overall trend of the data values, as indicated by the correlation

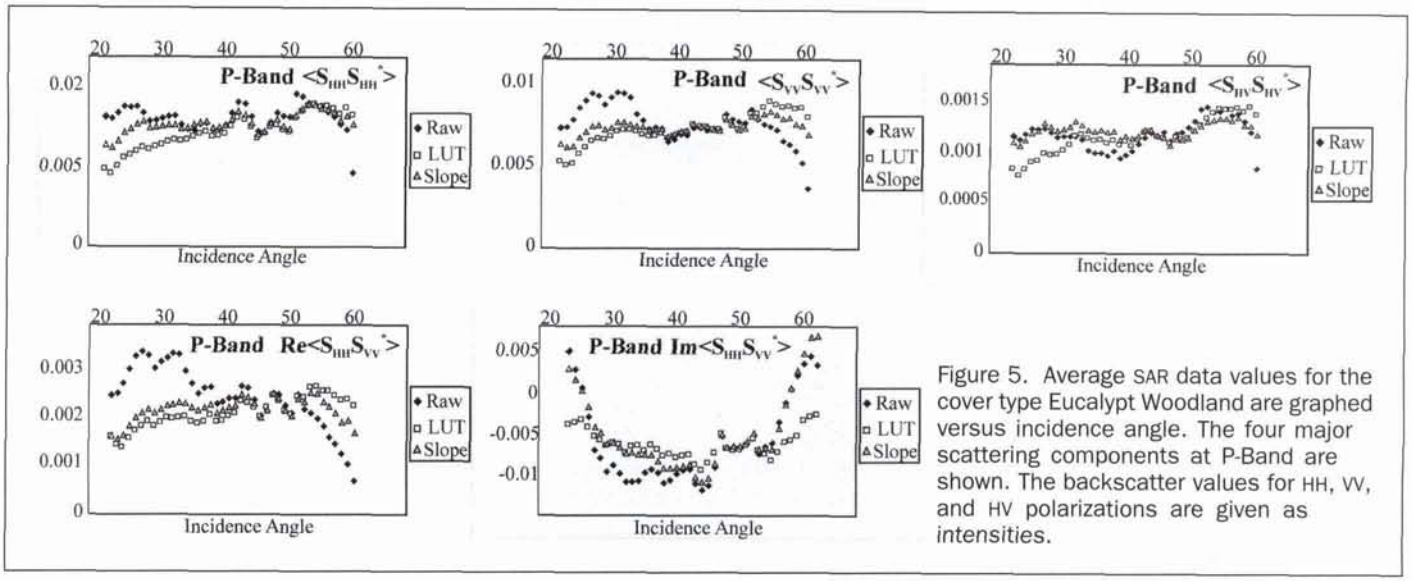

Figure 5. Average SAR data values for the cover type Eucalypt Woodland are graphed versus incidence angle. The four major scattering components at P-Band are shown. The backscatter values for HH, VV, and HV polarizations are given as *intensities*.

TABLE 5. THE CORRELATION COEFFICIENTS AND SLOPE FOR THE LINEAR REGRESSION OF P-BAND SAR DATA VERSUS INCIDENCE ANGLE FOR TWO DOMINANT LAND-COVER TYPES OF THE STUDY AREA.

E. Woodland Communities at P-Band

Scattering Element	Raw Data		LUT Method		Line-of-Best-Fit Method		Slope Method	
	r	slope	r	slope	r	slope	r	slope
$\langle S_{HH}S_{HH}^* \rangle$	−0.14	−0.006377	0.92	0.058877	0.93	0.068813	0.69	0.020856
$\langle S_{VV}S_{VV}^* \rangle$	−0.61	−0.040857	0.89	0.047477	0.87	0.045077	0.62	0.016004
$\langle S_{HV}S_{HV}^* \rangle$	0.35	0.016986	0.91	0.056082	0.90	0.054010	0.37	0.008932
$Re\langle S_{HH}S_{VV}^* \rangle$	−0.83	−0.000046	0.89	0.000024	0.83	0.000024	0.34	0.000007
$Im\langle S_{HH}S_{VV}^* \rangle$	0.31	0.000013	−0.03	0.000000	0.24	0.000007	0.25	0.000010

Floodplain at P-Band

Scattering Element	Raw Data		LUT Method		Line-of-Best-Fit Method		Slope Method	
	r	slope	r	slope	r	slope	r	slope
$\langle S_{HH}S_{HH}^* \rangle$	0.24	0.012704	0.77	0.078427	0.80	0.090769	0.56	0.039356
$\langle S_{VV}S_{VV}^* \rangle$	−0.44	−0.026644	0.79	0.060548	0.77	0.060085	0.58	0.029687
$\langle S_{HV}S_{HV}^* \rangle$	0.53	0.030200	0.77	0.070545	0.77	0.069813	0.43	0.021690
$Re\langle S_{HH}S_{VV}^* \rangle$	−0.50	−0.000029	0.77	0.000040	0.77	0.000039	0.55	0.000023
$Im\langle S_{HH}S_{VV}^* \rangle$	0.22	0.000012	−0.18	−0.000006	0.07	0.000002	0.13	0.000006

coefficient and slope of a first-order fit. These parameters are variable and do not give a clear indication of any method being superior to the raw data, especially for the cover type Floodplain. The graphical representation indicates that both correction methods improve the relationship for the real part of the HHVV co-polarized return, and the LUT method results in a significant reduction of the peaks observed in the very near and far range for the imaginary part of the co-polarized return.

The graphical results for the evaluation procedure performed using pixels allocated to the class of Floodplain according to the Landsat TM classification are shown in Figure 6 for four selected channels. These data contain far greater "random" variation, which obscures the overall trend to some degree. The behavior of the correction methods, as discussed for the data obtained for the land-cover type Eucalypt Woodland, holds for this cover type in relation to the overall trend in the data. The random variation observed is replicated by both correction methods.

Plate 1 is a color composite image of the P-HH, L-VV, and C-HV channels as raw and corrected data. The correction of these channels was based on the Slope method. The incidence angle contamination is very obvious in the near range of the data as an increased brightness obscuring the identification of ground features. Comparison to the corrected data visually demonstrates the effectiveness of this method for these data. The two largest land-cover components in this study area, *Eucalypt* open forest and Floodplain, can be clearly seen, as well as Mangroves along the saline creek environments.

The incidence angle correction procedure applied to the data allowed the use of a standard image classification algorithm for land-cover discrimination with high accuracy across the whole swath width of the AirSAR strip (Plate 2). An overall classification accuracy of 86.79 percent was achieved for nine land-cover classes, with a Kappa coefficient of 0.85. The associated error matrix derived from a total of 424 ground data points is shown in Table 6. The classification demonstrates that AirSAR is capable of discriminating between the following vegetation communities in the study area: Mangroves, *Melaleuca* Open Forest, Pine Forest, *Eucalypt* Forest/Open Forest, *Eucalypt* Woodland, and Closed/Riparian Forest. The lowest

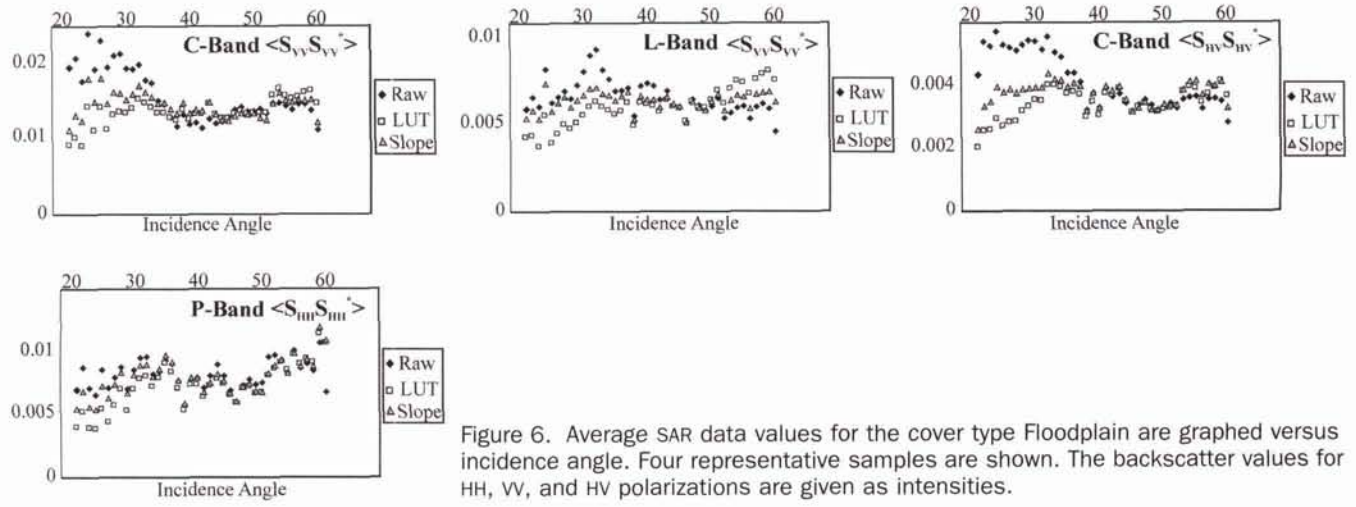

Figure 6. Average SAR data values for the cover type Floodplain are graphed versus incidence angle. Four representative samples are shown. The backscatter values for HH, VV, and HV polarizations are given as intensities.

TABLE 6. CONFUSION MATRIX FOR THE LAND-COVER CLASSIFICATION OF INCIDENCE ANGLE CORRECTED AIRSAR DATA

Image \ Ground Data	1	2	3	4	5	6	7	8	9	Total	PA [%]
1:E. Op Forest & Forest	**76**	4	.	.	.	3	.	.	.	83	91.6
2:E.Woodland	3	**35**	.	.	4	1	.	.	.	43	81.4
3:Closed Forest	1	.	**28**	1	1	2	.	.	.	33	84.8
4:Pine	.	.	1	**29**	.	.	.	.	.	30	96.7
5:Melaleuca Open Forest	4	4	2	.	**25**	.	.	.	.	35	71.4
6:Mangroves	.	4	2	.	.	**25**	.	.	.	31	80.6
7:Floodplain/Inundated Areas	.	1	1	.	.	1	**71**	6	.	80	88.8
8:Bare Soil/Grassland	.	.	.	.	2	.	8	**64**	.	74	86.5
9:Water	.	.	.	.	.	.	.	.	**15**	15	100.0
Totals	84	48	34	30	32	32	79	70	15	**424**	
									Overall Accuracy:		86.79
									Kappa Coefficient:		0.85

class accuracy was obtained for the *Melaleuca* communities, with 71.4 percent. Considerable overlap occurred with the Eucalypt woodland and open forest communities. The ground-truth data were collected by noting the tree density as well as the dominant species. Whether a Eucalypt community was dominated by Eucalyptus *miniata, tetrodonta*, or *bleeseri* was, however, not reflected in the analysis of the AirSAR data using the methodology described. Because structural differences between these tree species is minimal, this result was to be expected. The ability to differentiate the species *Melaleuca*, even at a lower success rate, is most likely due to this species inhabiting swamps and floodplains and often growing in uniform stands.

Bare Soil/Grassland, Water, and Floodplain could also be identified. The floodplain showed very distinct backscatter responses and required several training areas to be adequately mapped. Unfortunately, there is no ground data available to associate these areas with a particular land cover. The area mapped as Mimosa within the floodplain region is an exception because an aerial mapping survey had been undertaken and qualitatively confirms the existence and extent of this class.

Discussion

The Line-of-Best-Fit and the Slope correction methods proposed here depend on the linear relationship between azimuth and norm line. It has been shown that the sorted data values of azimuth lines exhibit a strong linear relationship to the norm line using sample lines in the near and far range. The similarity of results using the LUT and Line-of-Best-Fit correction method provide confirmation that this relationship holds for all azimuth lines. There is, however, a non-linearity at low data values when azimuth lines with high incidence angles are compared to the norm line (see Figure 2). These are presumed to be caused by the greater proportion of the land cover type Floodplain in the far range in comparison to the norm line. The greater proportion of low backscatter intensities in one line relative to the other not only causes this non-linearity, but also causes a variation in the slope and intercept of the regression line. Because the correction method utilizes these parameters, an error is introduced. No means for assessing the boundaries of validity for the correction method have been proposed. An assessment about the validity of the assumption, that the individual azimuth lines contain approximately equal proportions of the major land-cover types, must be made by the analyst using existing field knowledge. Conceptually, this is similar to assessing whether a histogram equalization can be used for the relative radiometric calibration of two adjacent or multi-temporal remotely sensed images.

The Slope method uses only the slope of the regression line to perform the correction and was shown to be the most successful for the magnitude of HH, VV, and HV backscatter components at the C and L Bands. The changes in SAR data observed with changing incidence angles in the sorted frequency data are determined by the effect of incidence angle as well as by pro-

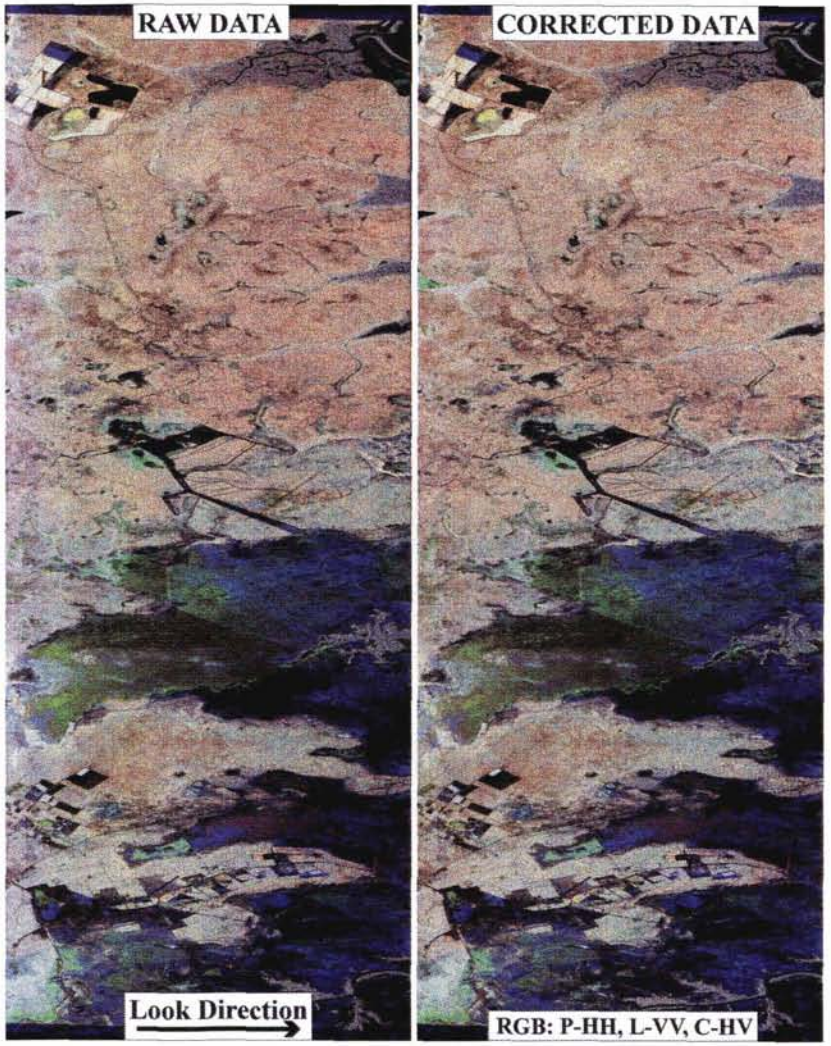

Plate 1. Color composites of P-HH, L-VV, and C-HV (as RGB) showing the raw (left) and corrected (right) AirSAR data of the study area. The incidence angle contamination can be seen clearly in the near range.

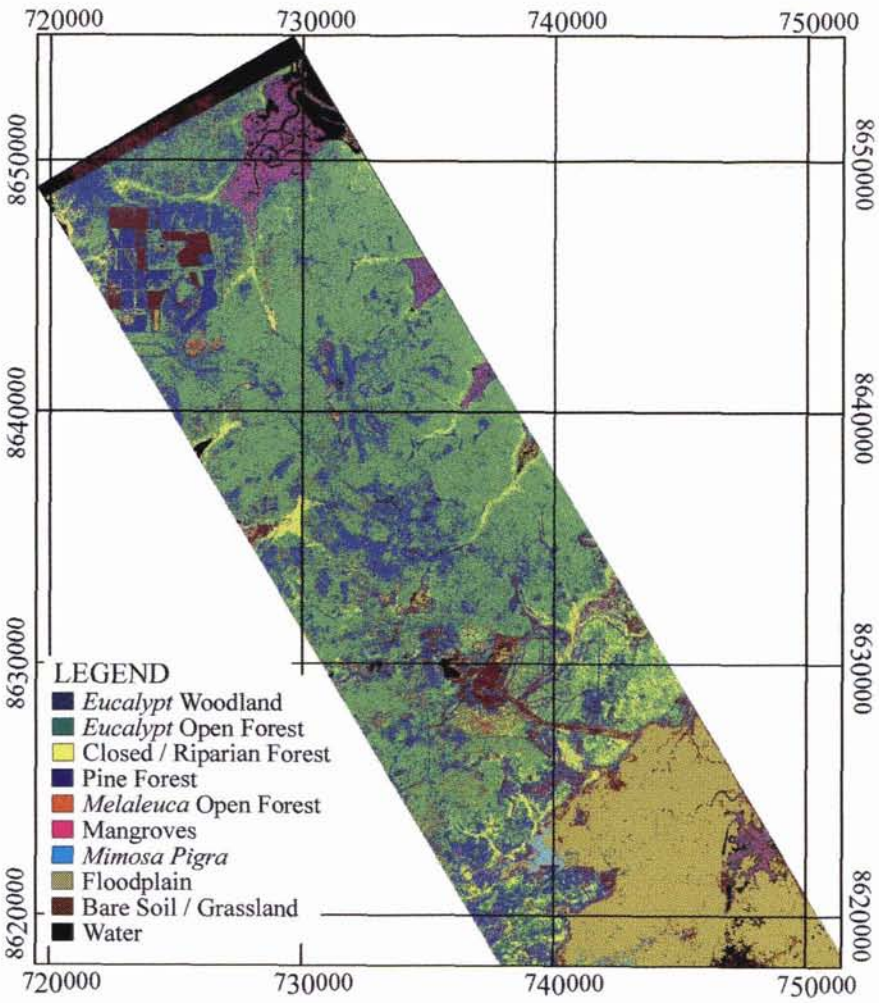

Plate 2. Land-cover classification of the incidence angle corrected AirSAR data.

portional changes in land-cover composition. If the proportions of land cover were equal in the respective azimuth lines, then a linear regression between the sorted values of these two azimuth lines should pass through the origin and, if the incidence angle effect was not present, the slope should equal one. Small variations in land-cover composition appear as localized distortions of the line of best fit and thus have greater impact on the intercept than the overall slope. The changes in SAR data due to changing incidence angle affect the data over their full range. This alters the slope of the line of best fit without significantly affecting the intercept. Using the slope of the line of best fit for the correction procedure is, therefore, a method less sensitive to variations in land cover across the range than are the other two methods.

The extracted data values for the cover type Floodplain show high frequency variation which is unlikely to be related to incidence angle due to its "noise"-like appearance. This variation is likely to be caused by the radar "seeing" the cover as much more diverse than does the optical sensor. The areas associated with the land-cover type Floodplain are spectrally similar within the frequency range employed by Landsat TM. SAR data, on the other hand, are sensitive to surface parameters such as surface roughness and variation in soil moisture content, which cause significant variability within this cover type. This was borne out in the classification process where a number of training areas was required for the identification of the floodplain. Unfortunately, no ground data are currently available to associate floodplain cover types with these distinct SAR classes. Research on SAR data for the discrimination of grasses and segdes in a floodplain environment is in progress with highly promising results. The high frequency fluctuations are thus attributed to the land-cover type containing a greater range of variability than is suggested by the optical sensor data. The similarity of the performance of the correction procedures to that observed using the Eucalypt Woodland communities as an indicator can be observed in the overall trend of the data despite this variation. The replication of the high-frequency variation by the correction method is an indication that valid information is not lost in the procedure.

The LUT method, or using the slope and intercept of the regression line, produced better or equal results for the real and imaginary components of the co-polarized returns at the C, L, and P Bands. In some instances, the Slope method performed equally well, but in many cases it produced inadequate results in the near and far range. Further research is required to determine the reason for this result.

The proposed incidence angle correction procedure will not be applicable to areas where changes in proportional land cover within azimuth lines of the SAR data are more pronounced. Further study will be required to refine the methodology for such cases. It may be possible to identify a range of SAR data values from the image data that are present in all azimuth lines in a sufficient quantity to derive the slope parameter. The positioning of the flight line determined by the analyst who has knowledge of the ground cover in the study area can play a crucial role in insuring that the assumption of approximately equal land-cover distributions within azimuth lines is met. If, for example, data are acquired in a coastal region, the a flight line perpendicular to the coast is more likely to satisfy this assumption than a line parallel to the coast.

The classification of the study area has shown that a standard image classification algorithm can be implemented on the corrected AirSAR data to discriminate land cover over the whole range of incidence angles with high accuracy. Vegetation communities could be discriminated according to density classes (Open Forest versus Woodland) as well as species, providing that sufficient structural difference exists. The ability to map *Mimosa Pigra* has to be investigated further because this initial assessment appears highly promising. Optical data are difficult to use for this purpose because this cover type exhibits spectral overlap with Mangroves, Closed Forest, and Eucalypt communities, depending on the growth stage (Menges, 1996). The potential stratification of AirSAR data for land-cover discrimination within the floodplain also requires further research. Again, optical data are limited because there is far less variation of the signal and because it cannot be used to monitor the immense seasonal variation due to cloud cover during the wet season.

Conclusion

SAR data are a promising tool to obtain remotely sensed information on land cover in addition to data obtained from optical sensors. The side-looking nature of the instrument introduces significant variation in incidence angle from an airborne platform. This not only causes geometric distortions but also variation in the scattering components measured. The changes introduced by variation in incidence angle are dependent on the land cover and can, therefore, not be removed by mathematical modeling unless the exact ground-cover composition is known. The proposed methods for the removal of this effect are based on the statistical comparison of lines of data with constant incidence angle. For the backscatter intensities at the various polarizations and frequency bands available, the use of the slope of a regression line between azimuth lines has been shown to achieve a successful correction even if there is some variation in the proportions of land cover present in azimuth lines at different incidence angles.

The removal of the effect of incidence angle variation is significant because it allows the use of standard classification techniques for the corrected data with high accuracy. Previous research attempting classification of land cover from SAR data has in the main relied on the assumption that the effect is minimal within an incidence angle range of 10 degrees and has, therefore, limited the study areas to this extent. This severely limits the utility of the data set as a whole. For satellite-borne SAR instruments, the variation of incidence angles across the range of the scene is negligible. Variations must, however, be taken into account for areas with significant topography. The methods presented here could be adapted to correct these effects if a sufficiently accurate digital elevation model were available.

Acknowledgments

The authors would like to acknowledge the financial assistance of the Cooperative Research Centre for the Sustainable Development of Tropical Savannas and the Department of Primary Industries and Fisheries for the provision of aerial survey data of *Mimosa Pigra* infestations. The project was carried out as part of the 1996 AirSAR mission in the Pacific Rim and contributes to the research effort of the CRC.

References

Ahmad, W., G.J.E. Hill, A.P. O'Grady, and C. Menges, 1998. Use of Multispectral Scanner Data for the Identification and Mapping of Tropical Forests of Northern Australia, *Asian-Pacific Remote Sensing Journal*, 11(1):13–22.

Baker, J.R., P.L. Mitchell, R.A. Cordey, G.B. Groom, J.J. Settle, and M.R. Stileman, 1994. Relationship between Physical Characteristics and Polarimetric Radar Backscatter for Corsican Pine Stands in Thetford Forest, U.K., *International Journal of Remote Sensing*, 15:2827–2849.

Bertuzzi, P., D. Vidal-Madjar, and M. Autret, 1992. The Use of a Microwave Backscatter Model for Retrieving Soil Moisture over Bare Soil, *International Journal of Remote Sensing*, 13:2653–2668.

Champion, I., 1996. Simple Modelling of Radar Backscattering Coefficient over a Bare Soil: Variation with Incidence Angle, Frequency and Polarization, *International Journal of Remote Sensing*, 17:783–800.

Chavez, P.S., Jr., and D.J. MacKinnon, 1994. Automatic Detection of Vegetation Changes in the Southwestern United States using Remotely Sensed Images, *Photogrammetric Engineering & Remote Sensing*, 60(5):571–583.

De Grandi, G.F., G.G. Lemoine, H. De Groof, C. Lavalle, and A.J. Sieber, 1994. Fully Polarimetric Classification of the Black Forest MAESTRO 1 AIRSAR Data, *International Journal of Remote Sensing*, 15:2755–2775.

Dobson, M.C., F.T. Ulaby, T. LeToan, A. Beaudoin, E.S. Kasischke, and N. Christensen, 1992. Dependence of Radar Backscatter on Coniferous Forest Biomass, *IEEE Transactions on Geoscience and Remote Sensing*, 30:412–416.

Dong, Y., B. Forster, and A. Milne, 1998. Segmentation and Classification of Single/Multi-Channel Radar Imagery Using Gaussian Markov Random Model, *Proceedings, 9th Australasian Remote Sensing and Photogrammetry Conference*, 20–24 July, Sydney, Australia, Paper No. 96 (CD-Rom).

Du, L., and J.S. Lee, 1996. Fuzzy Classification of Earth Terrain Covers Using Complex Polarimetric SAR Data, *International Journal of Remote Sensing*, 17:809–826.

Engman, E.T., 1991. Application of Microwave Remote Sensing of Soil Moisture for Water Resources and Agriculture, *Remote Sensing of Environment*, 35:213–226.

Henderson, F.M., and A.J. Lewis, 1998. *Principles & Application of Imaging Radar: Manual of Remote Sensing, Volume 2, Third Edition*, John Wiley & Sons, New York, N.Y., 866 p.

Hess, L.L., J.M. Melack, S. Filoso, and Y. Wang, 1995. Delineation of Inundated Area and Vegetation along the Amazon Floodplain with the SIR-C Synthetic Aperture Radar, *IEEE Transactions on Geoscience and Remote Sensing*, 33:896–904.

Hickey, S.H., 1985. *Northern Territory Geological Survey*, Department of Mines and Energy, Darwin, Australia, 22 p.

Hussin, Y.A., R.M. Reich, and R.M. Hoffer, 1991. Estimating Slash Pine Biomass Using Radar Backscatter, *IEEE Transactions on Geoscience and Remote Sensing*, 29:427–431.

Israelsson, H., J. Askne, and R. Sylvander, 1994. Potential of SAR for Forest Bole Volume Estimation, *International Journal of Remote Sensing*, 15:2809–2826.

Jensen, J.R., 1986. *Introductory Digital Image Processing, A Remote Sensing Perspective*, Prentice-Hall, Englewood Cliffs, New Jersey, 379 p.

Lemoine, G., G.F. Grandi, and A.J. Sieber, 1994. Polarimetric Contrast Classification of Agricultural Fields Using MAESTRO 1 AIRSAR Data, *International Journal of Remote Sensing*, 15:2851–2869.

Lin, D.S., E.F. Wood, K. Beven, and S. Saatchi, 1994. Soil Moisture Estimation over Grass-Covered Areas Using AirSAR, *International Journal of Remote Sensing*, 15:2323–2343.

Menges, C., W. Ahmad, Z.H. Khwaja, and G.J.E. Hill, 1996. Merging Minimum Distance to Mean and Maximum Likelihood Algorithms for Classifying *Mimosa Pigra* in Northern Australia, *Asian-Pacific Remote Sensing Journal*, 9:51–59.

Menges, C.H., J. Crerar, G.J.E. Hill, and W. Ahmad, 1998. A Method Estimating the Effect of Variation in Local Incidence Angle on AirSAR Data, *Proceedings of the Australasian Remote Sensing Photogrammetry Conference*, 20–24 July, Sydney, Australia, Paper No. 145 (CD-Rom).

Menges, C., W. Ahmad, G.J.E. Hill, and J.J. van Zyl, 1999. Evaluation of AirSAR Data for the Classification of Vegetation Communities in the Tropical Savannas of Northern Australia, *Proceedings, NARGIS*, 28–30 June, Darwin, Australia, CD-Rom Number 33.

Menges, C., J.J. vanZyl, G.J.E. Hill, and W. Ahmad, 2001a. A Procedure for the Correction of the Effect of Variation in Incidence Angle on AIRSAR Data, *International Journal of Remote Sensing*, (in press).

Menges, C., G.J.E. Hill, and W. Ahmad, 2001b. Use of Airborne Video Data for the Characterisation of Tropical Savannas in Northern Australia: The Optimal Spatial Resolution for Remote Sensing Applications, *International Journal of Remote Sensing*, (in press).

Ranson, K.J., and G. Sun, 1994. Northern Forest Classification Using Temporal Multifrequency and Multipolarimetric SAR Images, *Remote Sensing of Environment*, 47:142–153.

———, 1997. An Evaluation of AIRSAR and SIR-C/X-SAR Images for Mapping Northern Forest Attributes in Maine, USA, *Remote Sensing of Environment*, 59:203–222.

Rignot, E., and R. Chellappa, 1992. Segmentation of Polarimetric Synthetic Aperture Radar Data, *IEEE Transactions on Image Processing*, 1:281–299.

Rignot, E., J. Way, C. Williams, and L. Viereck, 1994a. Radar Estimates of Aboveground Biomass in Boreal Forests of Interior Alaska, *IEEE Transactions on Geoscience and Remote Sensing*, 32:1117–1124.

Rignot, E.J.M., C.L. Williams, J. Way, and L.A. Viereck, 1994b. Mapping of Forest Types in Alaskan Boreal Forests Using SAR Imagery, *IEEE Transactions on Geoscience and Remote Sensing*, 32:1051–1059.

Saatchi, S.S., J.V. Soares, and D.S. Alves, 1997. Mapping Deforestation and Land Use in Amazon Rainforest by Using SIR-C Imagery, *Remote Sensing of Environment*, 59:191–202.

Sun, G., and D.S. Simonett, 1988. A Composite L-Band HH Radar Backscattering Model for Coniferous Forest Stands, *Photogrammetric Engineering & Remote Sensing*, 54:1195–1201.

Sun, G., D.S. Simonett, and A.H. Strahler, 1991. A Radar Backscatter Model for Discontinuous Coniferous Forests, *IEEE Transactions on Geoscience and Remote Sensing*, 29:639–644.

Um, J., and R. Wright, 1999. 'Video Strip Mapping (VSM)' for Time-sequential Monitoring of Revegetation of a Pipeline Route, *Geocarta International*, 14:23–34.

van Zyl, J.J., and F.T. Ulaby, 1990. Scattering Matrix Representations for Simple Targets, *Radar Polarimetry for Geoscience Applications*, Artech House, Norwood, Massachusetts, pp. 17–52.

Wang, J.R., A. Hsu, J.C. Shi, P.E. O'Neill, and E.T. Engman, 1997. A Comparison of Soil Moisture Retrieval Models Using SIR-C Measurements over the Little Washita River Watershed, *Remote Sensing of Environment*, 59:308–320.

Wang, Y., J. Day, and G. Sun, 1993a. Santa Barbara Microwave Backscattering Model for Woodlands, *International Journal of Remote Sensing*, 14:1477–1493.

Wang, Y., F.W. Davis, and J.M. Melack, 1993b. Simulated and Observed Backscatter at P-, L-, and C-Bands from Ponderosa Pine Stands, *IEEE Transactions on Geoscience and Remote Sensing*, 31:871–879.

Wilson, B.A., P.S. Brocklehurst, M.J. Clark, and K.J.M. Dickinson, 1990. *Vegetation Survey of the Northern Territory, Australia*, Technical Report No. 49, Conservation Commission of the Northern Territory, Palmerston, NT, Australia, 117 p.

Zebker, H.A., and J.J. van Zyl, 1991. Imaging Polarimetry: A Review, *Proceedings of the IEEE*, 79:1583–1606.

Received 07 February 2000; accepted 28 March 2000; revised 28 April 2000